Analysis of Multicomponent Adsorption Kinetics on Activated Carbon

L. P. Ding and S. K. Bhatia
Dept. of Chemical Engineering, The University of Queensland, Brisbane, Qld. 4072, Australia

An integrated mathematical model for the kinetics of multicomponent adsorption on microporous carbon was developed. Transport in this bidisperse solid is represented by balance equations in the macropore and micropore phases, in which gas-phase diffusion dominates the mass transfer in the macropores, with the phenomenological diffusivities represented by the generalized Maxwell–Stefan (GMS) formulation. Viscous flow also contributes to the macropore fluxes and is included in the MS expressions. Diffusion of the adsorbed phase controls the mass transfer in the micropore phase, which is also described in a similar way by the MS method. The adsorption isotherms are represented by a new heterogeneous modified vacancy solution theory formulation of adsorption, which has proved to be a robust method for adsorption on activated carbons. The model is applied to the coadsorption and codesorption of C_2H_6 and C_3H_8 on Ajax and Norit carbon, as well as the displacement on Ajax carbon. The effect of the viscous flow in the macropore phase is not significant for the cases studied. The model accurately predicts the overshoot behavior and rollup of C_2H_6 during coadsorption. The prediction for the heavier compound C_3H_8 is always satisfactory, though at higher C_3H_8 mole fraction, the overshoot extent of C_2H_6 is overpredicted, possibly due to neglect of heat effects.

Introduction

Successful prediction of multicomponent adsorption kinetics is crucial for the design and optimization of adsorption and separation process. From a fundamental viewpoint, it is also one indication of the adequacy of the single-component equilibrium as well as kinetics model, and the predictive model for multicomponent equilibria that are incorporated in it.

Adsorption on activated carbon has attracted much attention, and has been the subject of much research because of its commercial importance. In this regard considerable effort has been devoted to the characterization of activated carbon and adsorption equilibrium of both the single- and multicomponent systems. However, there are only limited reports on kinetic modeling for multicomponent adsorption on activated carbon (Hu, 1992; Do and Do, 1998, 2000; Wang, 1998; Qiao and Hu, 2000). It is generally accepted that activated carbon has a porous structure consisting of pores of different size, ranging from fractions of a nanometer to several microns. This structure influences the transport of molecules inside the activated carbon, which occurs through multiple mechanisms. Proper consideration of all these mechanisms is essential for accurate prediction of the dynamic behavior on activated carbon, although in reality it is always simplified in one way or another (Yang, 1997).

A description of the adsorption kinetics of gaseous mixtures requires an adsorption isotherm to represent the adsorption equilibria of the multicomponent system on the specific adsorbent. The Langmuir isotherm combined with the ideal adsorbed solution theory (IAST) (Myers and Prausnitz, 1965), as well as several extensions for mixtures based on the Langmuir equation, are the most popular choices (Hu, 1992; Wang and Do, 1999; Kapteijn et al., 2000; Qiao and Hu, 2000; Delgado and Rodrigues, 2001). The disadvantage of the Langmuir isotherm is that it is thermodynamically consistent (Krichevskii, 1934; Rao and Sircar, 1999) only when the saturation capacities for all adsorbates are the same, which is not the case in most applications. Although the adoption of the IAST scheme can avoid this difficulty, the calculation becomes more complicated in comparison to the extensions of

Correspondence concerning this article should be addressed to S. K. Bhatia.

the Langmuir equation for mixture adsorption. Sundaram and Yang (2000) have compared the effect of two thermodynamically consistent isotherms, that is, multisite Langmuir equation and a modified Dubinin-type expression, on the theoretical effective diffusivities in diffusion of binary mixtures in zeolite, and obtained quite different results from these two isotherms. Generally, any thermodynamically consistent isotherm for multicomponent adsorption can be applied in the kinetic model; however, considerations of efficiency and accuracy of the predictive kinetic model limit the choices for the equilibrium models.

Another aspect to be addressed for mass transfer in multicomponent systems is the diffusion of gaseous and adsorbed phase mixtures in the particular solids. The emphasis here is the description of the cross-term diffusivities, or the binary diffusivities between different species (Marutovsky and Bülow, 1987). The generalized Maxwell–Stefan (GMS) approach (Krishna, 1993a,b; Krishna and Wesselingh, 1997) has been well accepted and applied to various systems to determine diffusion in gaseous and liquid mixtures. It is assumed that the relative motion between individual species in a mixture must be caused by a driving force on every species. This driving force is balanced by the friction between this species and all other components in the mixture. Each of these friction contributions is considered to be proportional to the corresponding differences in the diffusion velocities. The formulation of GMS can be generalized by the following expression (Krishna and Wesselingh, 1997)

$$-\nabla\mu_i = R_g T \sum_{\substack{j=1 \\ j\neq i}}^{n} \frac{x_j(\boldsymbol{u}_i - \boldsymbol{u}_j)}{D_{ij}}, \quad i = 1, 2, \ldots, n \qquad (1)$$

The Maxwell–Stefan formulation is practically convenient for estimation of the counterdiffusion of the mixtures in both the macropore as well as micropore phases, especially for ternary or more components systems. Alternatively, a method based on the Onsager approach of irreversible thermodynamics has been proposed by Kärger and Bülow (1975) for binary systems. Along these lines, Yang and coworkers proposed a method to predict the cross-term surface diffusivity from single-component diffusivities (Yang et al., 1991; Chen and Yang, 1992; Chen et al., 1993, 1994). However, their model is only developed for homogeneous adsorbent, such as zeolite and carbon molecular sieves, and it is also difficult to extend to systems involving more than two components.

In recent years, molecular simulation methods, such as Monte Carlo and molecular dynamics approaches, have become more attractive with the developments in computer technology. However, the computational expense, especially with regard to the time required, is still an obstacle to its application. At present, calculations using molecular simulation are mainly restricted to simple molecules in pores of ideal geometry or in well-organized solids such as zeolites (Saravanan and Auerbach, 1997; Coppens et al., 1999; Sanborn and Snurr, 2001).

In this article, an integrated model for the adsorption kinetics of binary adsorbates on activated carbon is developed. The transport in the activated carbon consists of the gaseous diffusion in the macropores in parallel with the adsorbate diffusion in micropores. Simultaneously, there also exists the mass transfer between the gaseous and adsorbed phases in the micropores, which can be represented by a generalized formulation applicable to any arbitrary isotherm equation (Ding et al., 2002). The adsorption equilibrium is described by a modified heterogeneous vacancy solution model (Ding and Bhatia, 2002). This model is developed on a mass-action law basis and turns out to be identical with the multisite Langmuir equation (Nitta et al., 1984). The new model is thermodynamically consistent, and also maintains the simplicity of the original vacancy solution theory (VST) (Suwanayuen and Danner, 1980; Cochran et al., 1985) for multicomponent adsorption, which had an earlier counterpart in the Soviet literature (Bering et al., 1977; Yakubov et al., 1977). In the kinetic model, the diffusion in the macropore phase and the adsorbed phase is represented by the Maxwell–Stefan (MS) approach for multicomponent mass transfer. In the development of the MS method for the diffusion of n components in the adsorbed phase, or surface phase, as described in the original work (Krishna, 1990; Krishna and Wesselingh, 1997), the vacant site is treated as the $(n+1)$th component of the system and included in the formulation, which is exactly the same assumption as in the vacancy-solution theory (Suwanayuen and Danner, 1980), as well as our modified VST model (Bhatia and Ding, 2001). This conceptual consistency with the MS approach makes the modified VST (Ding and Bhatia, 2002) especially attractive for modeling multicomponent adsorption kinetics. The original VST method had been criticized for lack of thermodynamic consistency (Talu and Myers, 1988), and had, therefore, been largely abandoned.

Theory

Adsorption equilibrium of mixtures on activated carbon

The heterogeneous modified VST model (HMVST) for adsorption on activated carbon has been developed and tested for the adsorption of different hydrocarbons on various activated carbons (Ding and Bhatia, 2002). Fundamentally, this isotherm is developed on the basis of a mass-action law to overcome the shortcoming of the original VST formulation. It turns out to be similar to the multisite Langmuir model (Nitta et al., 1984), formulated from the statistical thermodynamic analysis. The incorporation of pore-size-dependent energy broadens the applicability of this isotherm to heterogeneous adsorbents, such as activated carbon. Although the ethane/propane mixture studied in this work is almost ideal, even for heterogeneous surfaces, the IAST approach (Myers and Prausnitz, 1965) was not adopted because of the lengthy computational time. The authors have studied binary adsorption equilibria of various hydrocarbons in four different carbons, and found that the HMVST model can predict binary equilibria at least as accurately as the IAST can, but with substantially less computing time (Ding and Bhatia, 2002). Consequently, the HMVST model was used in this work, as discussed below.

The overall adsorption isotherm for species i can be represented by

$$C_i(P,T) = \int_0^{\infty} \frac{C_{\infty}}{\nu_i} \cdot \theta_i(P,T,H) \cdot f(H)\, dH \qquad (2)$$

where the local equilibrium in a single micropore of width H follows (Ding and Bhatia, 2002)

$$\frac{\theta_i}{\left(1-\sum_{j=1}^{n}\theta_j\right)^{\nu_i}} = \frac{\nu_i y_i P e^{-(\phi_i(H))/(R_g T)}}{C_\infty R_g T} \tag{3}$$

For slit-shaped micropores in activated carbon, H is defined as the distance between centers of the surface layers in opposite walls. The micropore-size distribution is assumed to be a gamma function, following

$$f(H) = \frac{q^{\gamma+1} H^{\gamma} e^{-qH}}{\Gamma(\gamma+1)} \tag{4}$$

The potential energy of the adsorbate molecule and a single wall of carbon is represented by Steele's 10-4-3 potential (Steele, 1973), from which the adsorbate–adsorbent interaction potential $\phi_i(H)$ in Eq. 3 is expressed by

$$\begin{aligned}\phi_i(H) &= \frac{5}{3}\epsilon_{is}\left\{\left[0.4\left(\frac{\sigma_{is}}{Z_{m,i}}\right)^{10} - \left(\frac{\sigma_{is}}{Z_{m,i}}\right)^{4} - \frac{\sigma_{is}^4}{3\Delta(Z_{m,i}+0.61\Delta)^3}\right]\right. \\ &\quad + \left[0.4\left(\frac{\sigma_{is}}{H-Z_{m,i}}\right)^{10} - \left(\frac{\sigma_{is}}{H-Z_{m,i}}\right)^{4}\right. \\ &\quad \left.\left. - \frac{\sigma_{is}^4}{3\Delta(H-Z_{m,i}+0.61\Delta)^3}\right]\right\}\end{aligned} \tag{5}$$

Overall balances for micropore and macropore phases

It is generally accepted that activated carbon has a bimodal pore-size distribution and contains pores ranging from a few angstroms to several microns, as shown in Figure 1, which depicts the pore-size distribution of Norit carbon (Qiao, 2000). Experimentally there is no unambiguous division between the macropores and mesopores, and we, therefore, assume that there are two kinds of pores in activated carbon, that is, macropores and micropores, according to the transport mechanisms in pores of different dimensions. The adsorption mainly takes place in the micropores, while the macropores play a role in the transfer of adsorbate from the outer surface of the particle to the micropores. Therefore, the kinetic behavior of adsorption can be described by the simultaneous and correlated mass-balance equations in the two phases.

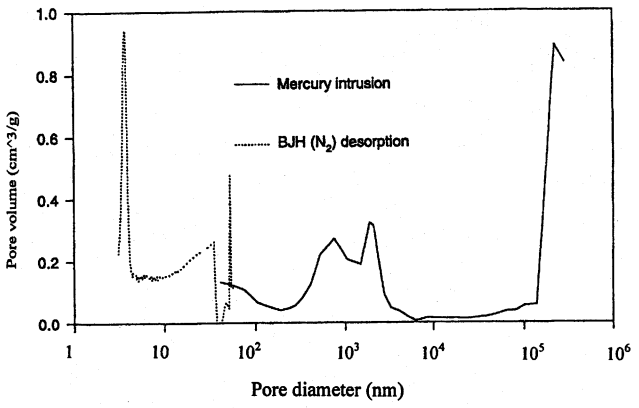

Figure 1. Pore-size distribution of Norit carbon (Qiao, 2000).

It is assumed that the concentration gradient at the microscale is negligible, and the microparticle-scale resistance for the adsorbed phase is, therefore, considered insignificant. The heat effect of sorption on the particle is also considered negligible and the system is assumed to be isothermal. Further, the model does not consider the external mass-transfer resistance as a very high gaseous flow rate is often used in experiments (Hu, 1992).

Micropore Phase. The mass-balance equation for species i in the micropore phase can be written as

$$(1-\epsilon_m)\epsilon_\mu \frac{\partial C_{\mu t,i}}{\partial t} = -\frac{1}{Z^a}\frac{\partial}{\partial Z}(Z^a N_i) + J_{m-\mu,i} \tag{6}$$

The diffusive flux N_i in the micropore phase over the particle scale is the summation of the local flux in every micropore and is represented by

$$N_i = \frac{1}{\tau_\mu}\int_0^\infty N_{p,i}(H) f(H)\, dH \tag{7}$$

The local flux of the adsorbed phase $N_{p,i}(H)$ can be derived from the force balance on the species. Following the approach of the generalized Maxwell–Stefan formulation (Krishna and Wesselingh, 1997), the force balance on the species i in a mixture of n adsorbates takes the form

$$-\frac{\nabla\mu_i}{R_g T} = \frac{V_i^D}{D_{\mu,i}} + \sum_{\substack{j=1\\ j\neq i}}^{n}\frac{\theta_j\left(V_i^D - V_j^D\right)}{D_{\mu,ij}} \tag{8}$$

The diffusive velocity can be expressed as

$$V_i^D = \frac{N_{p,i}^D}{C_i} \tag{9}$$

with

$$N_{p,i}^D = N_{p,i} - N_{p,i}^V \tag{10}$$

Substituting Eqs. 9 and 10 into Eq. 8 and after some rearrangement, the following expression is obtained

$$-\frac{C_{\mu,i}}{R_g T}\nabla\mu_i = \frac{N_{p,i}}{D_{\mu,i}} + \sum_{\substack{j=1\\ j\neq i}}^{n}\frac{C_{\mu,j}N_{p,i} - C_{\mu,i}N_{p,j}}{C_{\mu,t}D_{\mu,ij}} \tag{11}$$

in which it is assumed that there is no viscous flow in the adsorbed phase (Ding et al., 2002).

Equation 11 can be written in matrix form as

$$[B_\mu]\cdot\nabla\bar{\mu}=[A_\mu]\cdot\bar{N}_p \tag{12}$$

Its solution provides the adsorbed phase molar flux vector

$$\bar{N}_p=[L]\cdot\nabla\bar{\mu} \tag{13}$$

where $[L]=[A_\mu]^{-1}\cdot[B_\mu]$ is the phenomenological adsorbed phase diffusivity matrix, where $[A_\mu]$ and $[B_\mu]$ represent the effect of diffusive flow and viscous flow, respectively. Referring to Eq. 11, the elements of $[A_\mu]$ and $[B_\mu]$ are expressed by

$$A_{\mu,ik}=\begin{cases}\dfrac{1}{D_{\mu,i}}+\displaystyle\sum_{\substack{j=1\\ j\neq i}}^{n}\frac{\theta_j}{D_{\mu,ij}} & k=i\\ -\dfrac{\theta_i}{D_{\mu,ik}} & k\neq i\end{cases} \tag{14}$$

and

$$B_{\mu,kj}=-\frac{C_{\mu,k}}{R_gT}\delta_{kj} \tag{15}$$

The off-diagonal elements in $[A_\mu]$ represent the cross-correlation between different species, while the diagonal terms account for both the self-diffusion and the cross-correlation. It can be noticed from the preceding expressions that the phenomenological adsorbed-phase diffusivity matrix is closely related to the dimension of the micropores, as well as the surface coverage.

The chemical-potential gradient in the adsorbed phase can be expressed by

$$\frac{\partial\mu_i}{\partial Z}=R_gT\cdot\frac{1}{C_{me,i}}\cdot\frac{\partial C_{me,i}}{\partial Z} \tag{16}$$

Substituting the preceding expression together with Eqs. 7 and 13 into Eq. 6, it can be found that the independent variables in the left- and righthand sides of the equation are the concentrations in the adsorbed phase and the hypothetical equilibrium gaseous concentration, respectively. For convenience this hypothetical equilibrium gaseous concentration is chosen as the independent variable in the differential equation, and is related to the adsorbed-phase concentration by the adsorption isotherm, so that inversion of the isotherm is avoided. Consequently, the mass-balance equation (Eq. 6) can be represented by

$$\sum_{j=1}^{n}\left(\frac{\partial C_{\mu t,i}}{\partial C_{me,j}}\cdot\frac{\partial C_{me,j}}{\partial t}\right)=-\frac{1}{(1-\epsilon_m)\epsilon_\mu}\frac{1}{Z^a}\frac{\partial}{\partial Z}(Z^aN_i)+\frac{J_{m-\mu,i}}{(1-\epsilon_m)\epsilon_\mu} \tag{17}$$

Macropore Phase. The mass-balance equation for component i in the macropore phase can be written as

$$\epsilon_m\frac{\partial C_{m,i}}{\partial t}=-\frac{1}{Z^a}\frac{\partial}{\partial Z}(Z^aN_{m,i})-J_{m-\mu,i} \tag{18}$$

In the preceding expression, $N_{m,i}$ is the diffusion flux of species i in the macropores and can be derived in a similar manner to that in the adsorbed phase given in Eq. 13. It can be represented by

$$\bar{N}_m=-\frac{\epsilon_m}{\tau_m}[L_m]\cdot\nabla\bar{\mu}_m \tag{19}$$

where $[L_m]$ is given by

$$[L_m]=[A_m]^{-1}\cdot[B_m] \tag{20}$$

As in Eqs. 14 and 15, the matrices $[A_m]$ and $[B_m]$ are represented by

$$A_{m,ik}=\begin{cases}\dfrac{1}{D_{K,i}}+\displaystyle\sum_{\substack{j=1\\ j\neq i}}^{n+1}\frac{y_{m,j}}{D_{m,ij}} & k=i\\ -\dfrac{y_{m,i}}{D_{m,ik}} & k\neq i\end{cases} \tag{21}$$

and

$$B_{m,kj}=-\left(\frac{C_{m,j}}{R_gT}\delta_{kj}+\frac{C_{m,k}C_{m,j}}{D_{K,k}\eta_m}\cdot\frac{d_0^2}{32}\right) \tag{22}$$

The off-diagonal terms of $[A_m]$ account for the drag effect of the molecule–molecule collision between different species, while the diagonal elements represent the combined molecule–wall and molecule–molecule interaction. The molecular diffusivity is calculated by the Fuller correlation (Reid et al., 1987)

$$D_{m,ij}=\frac{0.00143T^{1.75}}{PM_{ij}^{0.5}(\Omega_i+\Omega_j)^2} \tag{23}$$

with $M_{ij}=2/(M_i^{-1}+M_j^{-1})$. Furthermore, macropores are assumed to be cylindrical in shape with diameter d_0, and the Knudsen diffusivity is estimated according to (Krishna and Wesselingh, 1997)

$$D_{K,i}=\frac{d_0}{3}\sqrt{\frac{8R_gT}{\pi M_i}} \tag{24}$$

The second term in Eq. 22 represents the viscous contribution to the macropore transport.

It should be pointed out that the total number of diffusing species in the macropore phase is $n+1$, in which the inert gas is taken into account. In the adsorbed phase the inert gas (normally nitrogen or helium) is omitted, as its adsorption is negligible.

Mass transfer between the macropore and micropore phases

The mass-transfer flux between the macropore and micropore phases, $J_{m-\mu,i}$, can be derived through a mass-exchange formulation generalizing the single-component case (Ding et al., 2002). Assuming no correlation between the interphase fluxes of different species, the mass-transfer rate for component i in a pore of width H can be represented by

$$j_{m-\mu,i} = k_{a,i}(H)a_{g,i}\left(\overline{C}_g\right)\phi_{v,i}\left(\overline{C}_\mu\right) - k_{d\mu,i}(H)C_{\mu,i}(H) \quad (25)$$

where $j_{m-\mu,i}$ is the transfer rate per unit area of intersection between macropores and micropores of width H, and $\phi_{v,i}$ is a representative function for the effective activity of the available adsorption space for component i and can be obtained from the equilibrium condition, leading to

$$\phi_{v,i}\left(\overline{C}_\mu\right) = \frac{k_{d\mu,i}(H)C_{\mu,i}(H)}{k_{a,i}(H)a_{ge,i}\left(\overline{C}_\mu\right)} \quad (26)$$

where $a_{ge,i}$ is the bulky activity of component i in equilibrium with the adsorbed concentrations. Substituting the preceding expression into Eq. 25, the transfer flux between the macropore and micropore phase in pores of size H can be approximated by

$$j_{m-\mu,i} = k_{d\mu,i}(H)C_{\mu,i}(H)\left[\frac{a_{g,i}\left(\overline{C}_g\right)}{a_{ge,i}\left(\overline{C}_\mu\right)} - 1\right] \quad (27)$$

Assuming ideality for the gas phase, the activity can be replaced by the concentration in the preceding equation. Therefore, the total mass-transfer rate per unit volume of the particle can be obtained by integration of Eq. 27 over the micropore volume distribution, as follows

$$J_{m-\mu,i} = \frac{S_s}{4\left(1-\epsilon_\mu\right)\left(1-\epsilon_m\right)}\int_0^\infty k_{d\mu,i}(H)C_{\mu,i}(H) \times\left(\frac{C_{m,i}}{C_{me,i}} - 1\right)f(H)\,dH \quad (28)$$

In deriving Eq. 28 we recognize that $f(H)/(1-\epsilon_m)$ represents the distribution of micropore cross-sectional areas intersecting the microphase surface per unit area of the latter. S_S is the macropore surface area per unit volume. Since this represents the area of that portion of the microphase surface that is not pierced by micropores, it follows that the total external microphase area is $S_S/4(1-\epsilon_\mu)$. Here the factor of 1/4 represents the projected fraction since the local macropore surface can be randomly oriented.

Micropore-size dependence of kinetic parameters

In our studies for the single-component sorption kinetics on activated carbon, we adopted the effective medium theory method (Kirkpatrick, 1973) to estimate the effective adsorbate diffusivity in the porous structure (Ding et al., 2002). While it has proved to be an efficient approach for complex structures, it is not readily applicable to the present case because of the difficulty in transforming the model in terms of independent pseudospecies. Consequently, the simpler averaging in Eq. 7 was used to estimate the fluxes.

The local adsorbed phase diffusivity of species i is given by

$$D_{\mu,i}(H) = D_{\infty,i}e^{-(b_iE_i(H))/(R_gt)} \quad (29)$$

where $E_i(H) = -\phi_i(H)$ and b_i is taken to be 0.5. Following the suggestion of Krishna (1990), the counterdiffusivity between two species in the adsorbed phase is estimated by the empirical Vignes relation, that is

$$D_{\mu,ij}(H) = \left[D_{\mu,i}(H)\right]^{\theta_i/(\theta_i+\theta_j)}\cdot\left[D_{\mu,j}(H)\right]^{\theta_j/(\theta_i+\theta_j)} \quad (30)$$

Therefore, the counterdiffusivity in the adsorbed phase is closely related to the adsorbed concentration of both components.

The local desorption rate constant is obtained as follows (Ding et al., 2002)

$$k_{d\mu,i}(H) = k_{d0,i}e^{-(E_i(H))/(R_gT)} \quad (31)$$

Boundary and initial conditions

The boundary conditions at the outer surface of the particle can be given by

$$k_{m,i}(C_{b,i} - C_{m,i}) = -(N_i + N_{m,i}) \quad (32)$$

and

$$-\frac{S_S}{4(1-\epsilon_m)(1-\epsilon_\mu)}N_i = J_{m-\mu,i} \quad (33)$$

At the center of the particle, the symmetry conditions are assumed, leading to

$$\frac{\partial C_{m,i}}{\partial Z} = 0, \qquad \text{at } Z = 0 \quad (34)$$

$$\frac{\partial C_{me,i}}{\partial Z} = 0, \qquad \text{at } Z = 0 \quad (35)$$

The initial conditions are

$$C_{m,i} = C_{m,i0} \quad (36)$$

$$C_{me,i} = C_{m,i0} \quad (37)$$

Solution Methodology and Application for Experimental Data

To solve the coupled partial differential equations, the constituent equations (Eqs. 17 and 18), together with the boundary and initial conditions given by Eqs. 32–37, are first transformed to a dimensionless form. Then the partial differential equations are transformed into ordinary differential

Table 1. Isotherm and Pore Structure Parameters for Ajax and Norit Carbons

Adsorbent	Adsorbate	$\delta_i \times 10^2$ (K^{-1})	ν_i^0	ϵ_{is} (kJ/mol)	q ($Å^{-1}$)	γ	$C_\infty \times 10^{-3}$ (mol·m^{-3})	d_o (Å)	τ_m
Ajax	C_2H_6	0.334	1.203	11.66e	3.97	39.4	20.9	8000	7.5
	C_3H_8	0.256	1.514	14.91e					
Norit	C_2H_6	0.402	1.336	12.43e	4.5	46.0	16.1	740	4.0
	C_3H_8	0.173	1.542	14.3e					

equations by discretizing the spatial coordinate using the orthogonal collocation method (Villadsen and Stewart, 1967). The resulting equations are solved by the differential algebraic system solver package (DASSL).

For validation of the model the sorption kinetics on Ajax carbon of C_2H_6 and C_3H_8 mixtures diluted in nitrogen at various temperatures and compositions were predicted and compared with the experimental data (Hu, 1992). The data include coadsorption and codesorption of C_2H_6 and C_3H_8, as well as the displacement of preadsorbed C_2H_6 by C_3H_8 and vice versa. The coadsorption and codesorption of C_2H_6 and C_3H_8 mixtures with helium as the inert gas at 303 K on Norit carbon were also predicted and compared with experimental results (Qiao and Hu, 2000). All the experimental results are presented in the form of the fractional uptake, which is the transient concentration normalized over the relevant equilibrium concentration, estimated according to

$$f_{a,i} = (a+1)\int_0^{R_0} Z^a \frac{\epsilon_m C_{m,i} + \epsilon_\mu (1-\epsilon_m) C_{\mu t,i}}{\epsilon_m C_{b,i} + \epsilon_\mu (1-\epsilon_m) C_{\mu 0,i}} dZ \quad (38)$$

The parameters of pore-size distribution function, as well as those of the adsorption isotherm for each adsorbate have been obtained from the equilibrium study of the same system (Ding and Bhatia, 2002) and thereafter are applied in this work. Table 1 lists the isotherm and pore-size distribution parameters for C_2H_6 and C_3H_8 on Ajax and Norit carbon obtained in this earlier study. The physical properties of Ajax and Norit carbon (Hu, 1992; Qiao, 2000) are also given in Table 1. The tortuosity for the macropore and micropore are taken to be the same, as applied in the single-component calculation. It can be noticed from the values given in Table 1 that these two carbons have similar micropore-size distribution; however, the macropore sizes are quite different.

For computing the multicomponent adsorption kinetics, the intrinsic adsorbed-phase mobility of component i far from the pore surfaces, $D_{\infty,i}$, as well as the gas–adsorbate phase exchange rate coefficient, $k_{d0,i}$, need to be determined from single-component adsorption kinetic data on the same carbon. In our earlier article dealing with the single-component kinetics (Ding et al., 2002), the micropore network transport was modeled using effective medium theory (EMT) (Kirkpatrick, 1973), which is somewhat more accurate than the pore-volume averaging in Eq. 7. The kinetic parameters for C_2H_6 and C_3H_8 on both carbons are listed in Table 2. However, it was found that the current approach gave essentially identical results for the single-component case, using the same values for the kinetic parameters $D_{\infty,i}$ and $k_{d0,i}$. As an example, Figure 2 depicts the experimental data for sorption of C_2H_6 and C_3H_8 on Ajax (Hu, 1992) and Norit carbon (Qiao and Hu, 2000), and the prediction based on the current approach as well as the prior EMT-based approach (Ding et al., 2002), using parameter values from the latter fits. The prediction results using the present model are displayed in Figure 2 by the dotted lines, together with the earlier fitted results as the solid lines. It is evident that these two methods produce nearly identical results, so that the earlier parameters can be reliably applied for the prediction of multicomponent adsorption kinetics of the corresponding adsorbates.

Results and Discussion

Application of the kinetic model to coadsorption of binary adsorbates

Figure 3 displays the coadsorption data of C_2H_6 and C_3H_8 on Ajax (Hu, 1992) and Norit (Qiao and Hu, 2000) carbons, as well as the model predictions based on the single-component parameters in Tables 1 and 2, determined earlier (Ding et al., 2002). For the data, the bulk pressure is 101.3 kPa. The more strongly adsorbed component C_3H_8 is the slow-diffusing species, and the roll-up phenomenon of C_2H_6 can, therefore, be observed from the coadsorption of C_2H_6 and C_3H_8. The model prediction for both carbons is acceptable, as shown in Figure 3. The model not only exhibits the roll-up behavior of the fast diffusing–weak adsorbing species, that is, C_2H_6 in the experiment, but also predicts the magnitude of the rollup and the time when it takes place.

It can be seen that at higher C_3H_8 concentration, the model overestimates the overshoot extent of C_2H_6, while the pre-

Table 2. Kinetic Parameters for C_2H_6 and C_3H_8 on Ajax and Norit Carbons

Adsorbent	T (K)	$D_{\infty,i} \times 10^6$ (m²·s^{-1})		$k_{d0,i} \times 10^6$ (m·s^{-1})		$D_{m,ij} \times 10^4$ (m²·s^{-1})	$D_{K,i} \times 10^4$ (m²·s^{-1})	
		C_2H_6	C_3H_8	C_2H_6	C_3H_8		C_2H_6	C_3H_8
Ajax	283	1.36	1.21	1.04	4.78	0.079	1.192	0.984
	303					0.089	1.233	1.018
	333					0.106	1.293	1.067
Norit	303	3.10	2.71	9.86	14.17	0.089	0.115	0.095
	333					0.106	0.12	0.099

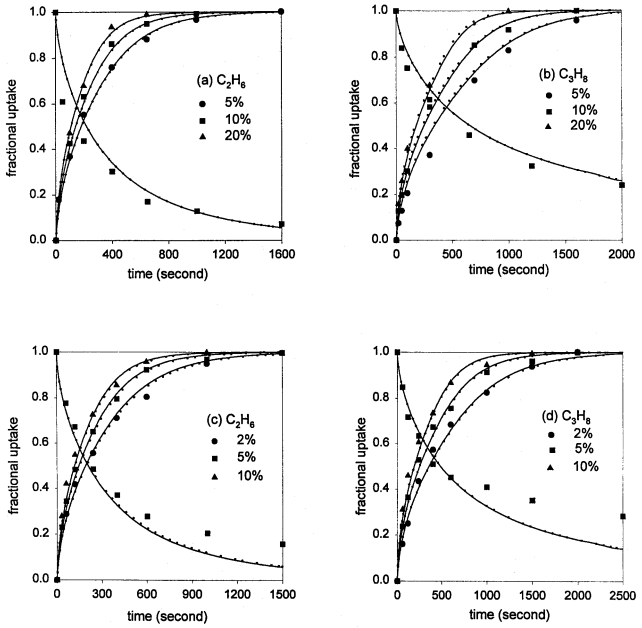

Figure 2. Model fitting and experimental uptake kinetic data at 303 K and 101.3 kPa on Ajax and Norit carbons.

Solid line represents the fitting result using EMT method, while the dotted line represents the prediction by current model using the EMT-fitted kinetic parameters. (a), (b) Sorption on Ajax carbon 4.4-mm slab; (c), (d) sorption on Norit carbon 8.82-mm slab.

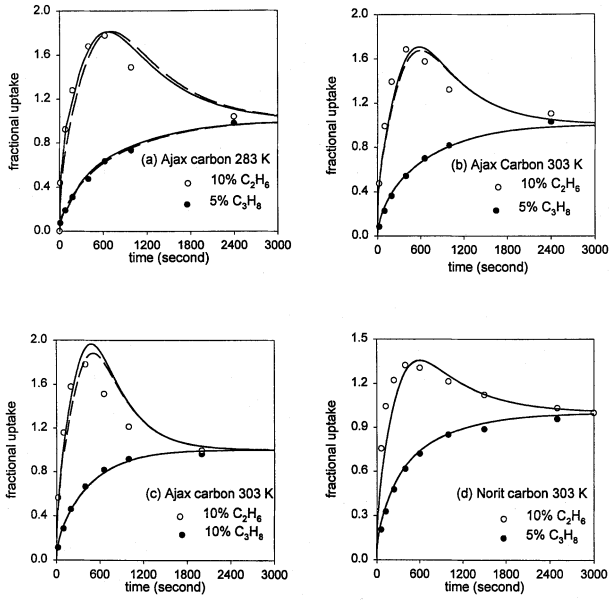

Figure 3. Experimental and predicted coadsorption uptake curve on Ajax carbon 4.4-mm slab and Norit carbon 8.82-mm slab.

The symbols represent experimental results. The solid line represents the predicted result considering viscous flow in macropore transport, while the dashed line represents the predicted result neglecting viscous flow.

diction for C_3H_8 compares well with the experiment. The reason for the deviation at higher C_3H_8 mole fraction may be due to the nonisothermal effect during adsorption. As the bulk concentration of C_3H_8 increases and the adsorption of C_3H_8 is enhanced, so is the heat produced from adsorption. The temperature increase resulting from the increases of C_3H_8 adsorption is larger than that from the C_2H_6 adsorption of the same amount, as the molar heat of adsorption for C_3H_8 is greater than that for C_2H_6. Therefore, the increase in C_3H_8 concentration in the gas mixture will result in a lower overshoot extent of C_2H_6 in the experiment, while the prediction with the isothermal assumption overestimates it, as shown in the uptake curves.

It is also found that the adsorption is faster at higher temperatures, as expected. The magnitude of C_2H_6 rollup decreases with an increase in temperature for the same composition. This is because the adsorbed amount decreases with the increase in temperature and the dragging effect of C_3H_8 on C_2H_6 decreases accordingly.

In general, from the comparison of experimental data with the model prediction for coadsorption of C_2H_6 and C_3H_8 at different temperatures, it can be concluded that the proposed model is well suited for quantitatively representing the adsorption and diffusion process of both compounds on activated carbon. The prediction result improves with decrease in the ratio of C_3H_8 to C_2H_6 mole fraction in the feed mixtures. The accuracy of the model prediction is also better at a lower temperature than at a higher temperature. The reason for this may be due to the nonisothermal effects in adsorption. The heat effect will result in less adsorption, and, therefore, will lower the overshoot degree of C_2H_6, as shown in Figure 3. As the amount adsorbed is decreased with temperature, the contribution of the adsorption heat becomes more significant, and the deviation of the model prediction for isothermal adsorption is more serious compared with the experimental data.

The solid lines in Figure 3 depict the predicted uptake curve when the viscous flux, represented through the second term in Eq. 22, is considered in the macropores. The viscosity of gas mixtures was estimated by the Wilke method, which is a simple extension of the kinetic theory approach to low-pressure multicomponent mixtures, as follows (Reid et al., 1987)

$$\eta_m = \sum_{i=1}^{N} \frac{y_i \eta_i}{\sum_{j=1}^{N} y_j \Phi_{ij}} \tag{39}$$

where Φ_{ij} is expressed by the Herning and Zipperer approximation, that is, $\Phi_{ij} = (M_i/M_j)^{0.5}$. The single-component viscosity was estimated by the Chapman–Enskog viscosity equation.

The viscous flow in the micropore phase is not included in the calculation, as the contribution from this term is negligible in comparison with the diffusive flux, based on the analysis for single-component adsorption kinetics (Ding et al., 2002). The dashed lines in Figure 3 represent the prediction results without viscous flow in the macropores. It can be seen that the prediction, including viscous flow, is slightly closer to the experimental data than that excluding the viscous term,

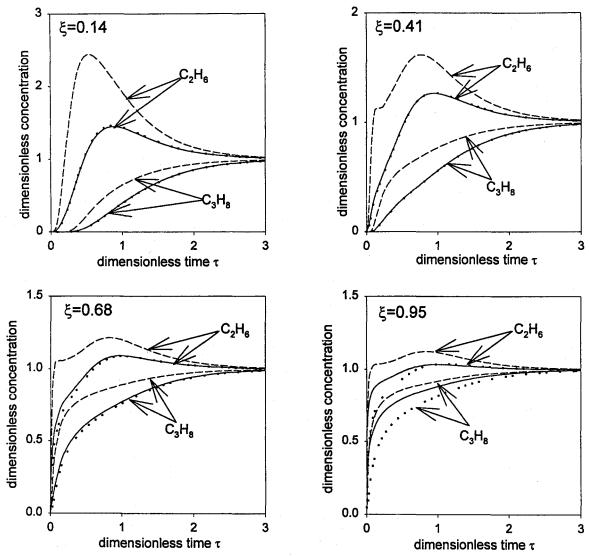

Figure 4. Intraparticle concentration profiles for binary adsorption.

Solid, dotted, and dashed lines represent the gas, adsorbate, and hypothetical equilibrium gas-phase concentration, respectively.

although both approaches can offer quantitatively acceptable results. The trend caused by the viscous flow as shown in Figure 3 is consistent with a previous study on the contribution of the viscous flow to the effective diffusivity in a porous media (Krishna, 1993). At the experimental conditions studied here, the neglect of viscous flux has little impact on the kinetic behavior of the adsorbates. Therefore, it is not considered in all the following calculations.

Intraparticle concentration profiles during adsorption

In order to observe the adsorption and mass-transfer process more closely, the intraparticle concentration profiles of the macropore gas phase, micropore adsorbate phase, as well as the hypothetical equilibrium gas phase are displayed in Figure 4. The spatial coordinate ξ is the dimensionless radial distance from the particle center, defined as $\xi = Z/R_0$.

The calculation is performed for a coadsorption of 5% C_2H_6 and 5% C_3H_8 on Ajax carbon of a 2.6-mm slab at 303 K. For the fast-moving/weak-adsorbing species, C_2H_6, there are peaks for the concentrations inside the particle. The front of the concentration peak is moving from the center to the surface of the particle. It can be found that the dimensionless times at which the maximum adsorbate concentration is reached are 0.892, 0.956, and 0.988 for ξ equal to 0.14, 0.41, and 0.68, respectively. This delay in proceeding to the surface of the particle can be explained as follows: C_2H_6 diffuses from the outer surface of the particle into the macropores swiftly, and simultaneously adsorption occurs in the micropores. The C_2H_6 continuously transfers into the particle until the maximum macropore concentration is reached at the center of the particle. At this moment, the concentration gradient for C_2H_6 from the particle center to the surface is negative, and C_2H_6 starts to diffuse outward. However, the heavy-component C_3H_8 keeps on diffusing into the particle and being adsorbed in the micropores. This results in the displacement of some adsorbed C_2H_6 by C_3H_8, as the latter is more strongly adsorbed than C_2H_6. The desorbed C_2H_6 contributes to the outward diffusive stream of C_2H_6 and increasingly delays the concentration peak of C_2H_6 in the macro-pores approaching the surface of the particle.

For the slow diffusing/strong adsorbing species, C_3H_8, the concentrations for the gas, adsorbate, and the hypothetical equilibrium phases monotonically increase with time. At the beginning of the adsorption process, however, there is no C_3H_8 in the inner part of the particle, as the diffusion is slow compared with C_2H_6. Figure 4b shows that there is no C_3H_8 in the gas or adsorbate phases at the vicinity of $\xi = 0.41$ until $\tau = 0.1$. However, for C_2H_6 the lag is only evident at $\tau = 0.01$ at $\xi = 0.14$, as C_2H_6 diffuses much faster than C_3H_8.

Figure 4 shows that the maximum of the hypothetical equilibrium concentration for C_2H_6 is synchronizing with the gaseous-phase concentration, but the buildup of the adsorbate phase concentration is faster than that of the gaseous phase. This demonstrates that both macropore and micropore diffusion controls the transport process, and that the mass-transfer resistance between the macropore and micropore phase is negligible. The lag in the macropore phase concentration becomes more evident toward the center of the particle. It implies that the adsorbed C_2H_6 has begun to be displaced by C_3H_8 though C_2H_6 continues to diffuse into the particle. Because of the nonlinearity of the isotherm, a small increase of C_3H_8 in the gaseous phase can cause a large decrease in the amount of C_2H_6 adsorbed. When C_2H_6 approaches the peak concentration in the adsorbate phase, the rate of concentration change is smaller than that in the initial stage. In contrast, the gaseous-phase concentration of C_3H_8 increases monotonically. Therefore, the adsorbate-phase concentration of C_2H_6 starts to decline in advance of the gaseous phase.

The hypothetical equilibrium concentration deviates from the macropore-phase concentration at the surface of the particle but not near the center. This is because the mass exchange is only important at the surface of the particle, where the macropore-phase concentration is high. In the particle interior the macropore and micropore resistance increases and the equilibrium concentration approaches the macropore concentration.

In general, the intraparticle concentration profile of gaseous and adsorbate phases indicates that both the macropore and micropore resistances are important for binary adsorption in bidisperse activated carbon. The MS formulation can describe the diffusivities in both the macropore and micropore phases.

It can be seen in Figure 4 that initially during adsorption, there is a rapid initial rise followed by some flattening-out in the adsorbate concentration of the weak adsorbing–fast diffusing species C_2H_6 near the surface of the particle. This is due to the nonzero initial concentration value applied in the calculation, and the absence of external mass-transfer resistance. The calculation experiences singularity difficulties when the initial adsorbate concentration is set to be zero. In practice the concentration therefore is assigned a small value, for example, 10^{-4} or less. However, perhaps even more important is the absence of mass-transfer resistance, which causes the surface concentration to abruptly increase, leading to very steep gradients in concentration. This can cause diffi-

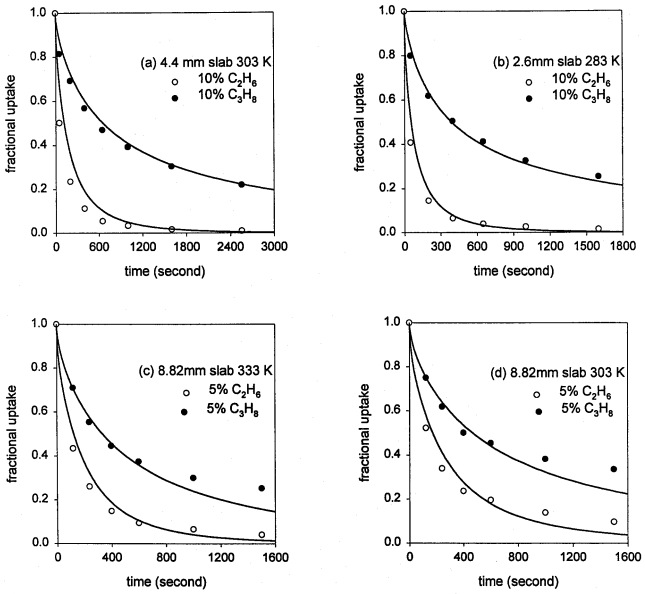

Figure 5. Experimental and predicted codesorption curve on Ajax and Norit carbon.

The symbols are experimental results. The solid line is the predicted result. (a), (b) Ajax carbon; (c), (d) Norit carbon.

culties with stiffness and instability of the solution near the surface during brief periods. However, the overall particle uptake dynamics did not show such effects, as seen in Figure 3.

Application of the kinetic model to codesorption of binary adsorbates

Next the codesorption of C_2H_6 and C_3H_8 from the equilibrated adsorbent by flushing with an inert gas are predicted and compared with the experimental data. Figure 5 displays the desorption curve of C_2H_6 and C_3H_8 on Ajax carbon (Hu, 1992), as well as Norit carbon (Qiao, 2000). In comparison with the experimental data, it is found that the proposed model can accurately predict the codesorption behavior of both adsorbates on Ajax carbon. In the codesorption process, there is no reverse flow of any compound, and the diffusion of both species is enhanced. In comparison with the single-component desorption curve in Figure 2, it can be found that the desorption rate of C_3H_8 is increased slightly by the existence of C_2H_6, while C_2H_6 desorption is accelerated significantly due to the codiffusion of C_3H_8. The diffusions of both compounds are in the same direction, and the friction of the heavier component, C_3H_8, on the lighter one, C_2H_6, has a much stronger effect than vice versa. Therefore, the increase in the diffusivity of C_2H_6 is more significant than that of C_3H_8.

In Figures 5c and 5d, the model overpredicts the codesorption on Norit carbon at later stages of the process. This is caused by the deviation of the fitting for single-component desorption on the Norit carbon, as shown in Figures 2c and 2d. It indicates that the accuracy of the kinetic parameters derived from the single-component sorption data is important for the successful prediction of binary adsorption kinetics.

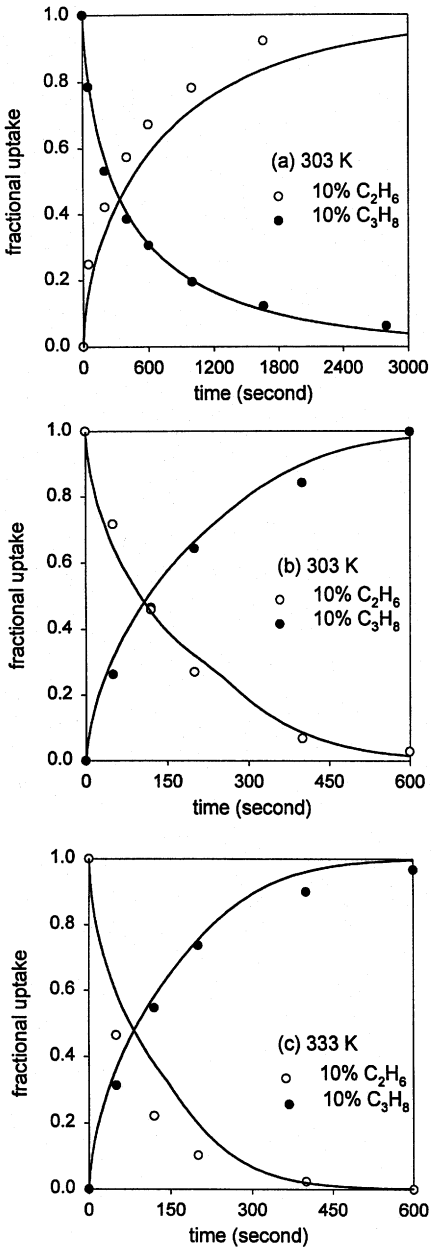

Figure 6. Experimental and predicted displacement curve on Ajax carbon 2.6-mm slab.

The symbols represent experimental results, and the solid lines the predicted results.

Application of the kinetic model to binary displacement

The proposed model is also applied to the displacement of one adsorbate preadsorbed on Ajax carbon by another compound (Hu, 1992). Figure 6a displays C_3H_8 of 10% mole fraction in a mixture with nitrogen in equilibrium in a 2.6-mm slab displaced by 10% C_2H_6 at 303 K. Figures 6b and 6c display C_2H_6 of 10% mole fraction in a mixture with nitrogen displaced by 10% C_3H_8 at 303 K and 333 K, respectively. Figures 6a and 6b show that the time scales to reach equilibrium are quite different for C_3H_8 displaced by C_2H_6 and C_2H_6 displaced by C_3H_8 with the same mole fraction for both species and at the same temperature. By comparison

with the single-component sorption kinetics of C_2H_6 and C_3H_8 in Figures 2a and 2b, it can be concluded that the displacement time largely depends on the adsorption or desorption time of single C_3H_8 at the same fraction. When C_3H_8 is displaced by C_2H_6, the time needed to reach equilibrium is close to the desorption time of single-component C_3H_8. For C_2H_6 displaced by C_3H_8 as well, the time is also close to the adsorption time of single C_3H_8. This observation reiterates the significant influence of the strongly adsorbed component on the adsorption kinetics of binary mixtures. The heavier species dominates the overall diffusion and kinetic process. From Figure 6, it can be seen that the proposed model can predict the kinetic behavior of both adsorbates very well, although there is some underestimation for the adsorption of C_2H_6 in the displacement of C_3H_8.

Comparison of predictions by different models

The predicted result using the proposed model is compared here with that obtained by different models. The models studied are the dual diffusion and finite kinetic model (Wang and Do, 1999), as well as the pore and surface diffusion in combination with IAST and micropore-size distribution model (Qiao and Hu, 2000). The model prediction for coadsorption of 5% C_2H_6 and 5% C_3H_8 at 283 K is displayed in Figure 7. Overall, the comparison indicates that the model proposed in this work produces the best result among all three approaches. The other two methods underpredict the roll-up magnitude of C_2H_6. In these two models, the adsorbed phase diffusivity was calculated using the Fickian approach, and the cross-term coefficients were neglected. Therefore, these models underestimated the dragging effect of the heavier compound on the lighter one and predicted a rollup less than the experimental observation. Although the application of the GMS formulation on the adsorbed phase diffusion, as well as the concentration dependence of the cross-term diffusivity represented by Eq. 30, requires more fundamental investigation, Figure 7 provides some support for the proposed kinetic model using the MS expression for diffusion in the adsorbed phase.

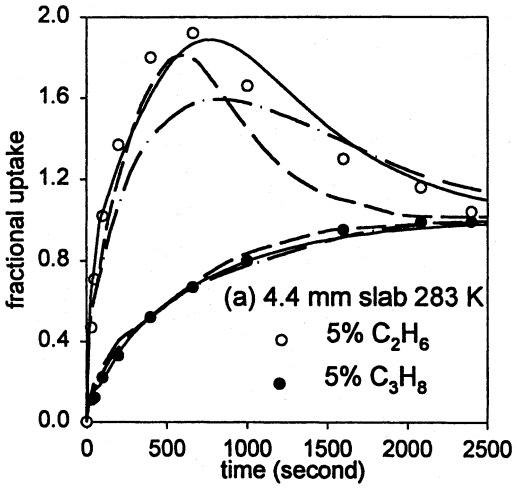

Figure 7. Comparison of predicted uptake curve of coadsorption on Ajax carbon by different kinetic models.

Symbols represent experimental results. The solid line is the predicted result using the current model, the dashed line represents the result of Qiao and Hu (2000), and the dash-dotted line the result of Wang and Do (1999).

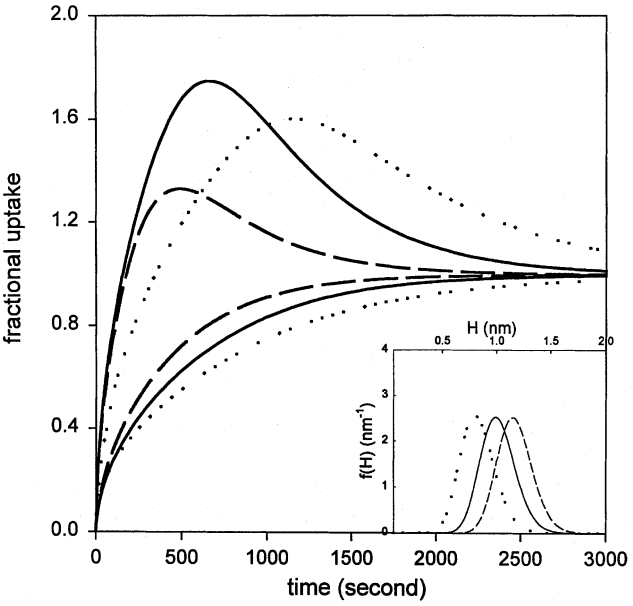

Figure 8. Effect of mean pore size on binary adsorption kinetics of C_2H_6 and C_3H_8 on activated carbon.

The dotted, solid, and dashed lines represent the model prediction for adsorption on carbon with mean pore size of 0.8 nm, 1.0 nm, and 1.2 nm, respectively. The inset depicts the corresponding pore-size distributions.

Effect of micropore heterogeneity on binary adsorption

Since the adsorption and micropore diffusion in activated carbon are closely related to the pore-size distribution of the adsorbent, the effect of micropore heterogeneity is investigated in terms of mean pore size and the spread of pore-size distribution. The calculation applies the isotherm and kinetic parameters on Ajax carbon as listed in Tables 1 and 2. Figure 8 displays the uptake curve of 5% C_2H_6 and 5% C_3H_8 adsorption on carbon of a 4.4-mm slab at 303 K with different mean pore sizes. The dotted and dashed lines display the uptake on adsorbents with mean micropore width of 0.8 nm and 1.2 nm, respectively. The solid line represents the uptake on Ajax carbon at the condition mentioned earlier. The gamma-function parameters q and γ are 33.25 and 26.6 to obtain a mean pore width of 0.8 nm, while they are 45.83 and 55.0 for a mean pore width of 1.2 nm. In doing so, the variance of pore-size distribution is constant.

For both adsorbates, the uptake curves indicate that with an increase of mean pore width, the time to reach adsorption equilibrium decreases. In other words, the adsorption becomes slower with a pore-size distribution shift to smaller pores. This is caused by the decrease in micropore diffusivities in the adsorbate phase. It has been found that for both compounds, the amount adsorbed at equilibrium increases with mean pore width increasing from 0.8 nm to 1.2 nm due to stronger interaction energy with the adsorbent. Therefore,

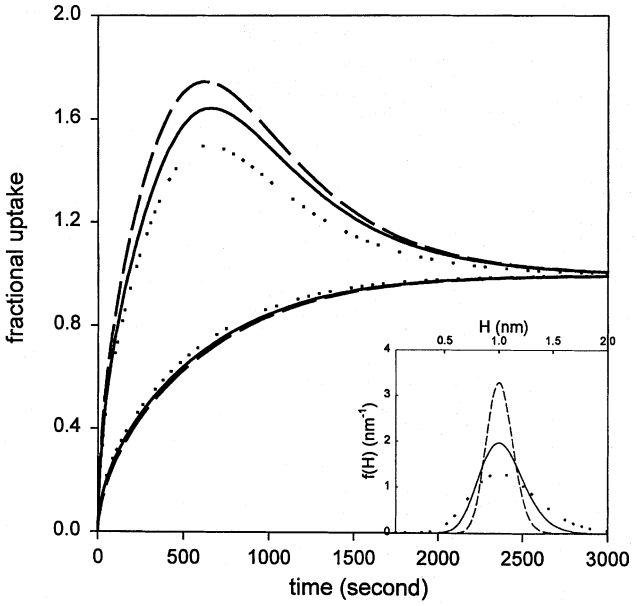

Figure 9. Effect of the spread of pore width on binary adsorption kinetics of C_2H_6 and C_3H_8 on activated carbon.

The dotted, solid, and dashed lines represent the predicted uptake for adsorption on carbon with pore-size distribution variance of 0.3, 0.2, and 0.12, respectively. The inset depicts the corresponding pore-size distributions.

the micropore diffusivity increases as well, according to Eq. 29 and the mass transfer speeds up remarkably.

It also can be seen in Figure 8 that the peak fractional uptake of C_2H_6 attains a maximum value at a mean pore width of 1.0 nm. This is due to the selective adsorption of C_3H_8 over C_2H_6 for this pore-size distribution. It has been found that the equilibrium selectivity of C_3H_8 over C_2H_6 is 7.56, 9.52, and 5.24 for a mean of 0.8 nm, 1.0 nm, and 1.2 nm, respectively. It indicates that the variation of the roll-up magnitude with mean pore width has the same trend as the equilibrium selectivity. The selective adsorption of the heavier compound will increase the diffusivity of the lighter one significantly, as it is highly related to the concentrations of both species. It, therefore, appears that the roll-up extent of C_2H_6 reaches its peak value at highest selectivity.

Figure 9 shows the effect of the spread of pore size on adsorption kinetics. The dashed, solid, and dotted lines represent the uptake on adsorbent of pore-size distribution with standard deviation of 0.12, 0.2, and 0.3, respectively. The mean pore width is maintained constant at 1.0 nm for all three cases. The calculation has shown that the equilibrium adsorption of C_2H_6 decreases when the distribution becomes narrower, while C_3H_8 is adsorbed more with a narrower pore-size distribution. Therefore the equilibrium selectivity of C_3H_8 over C_2H_6 increases monotonically with the decrease of the pore-size distribution variance. The change in roll-up magnitude with distribution variance also follows the same trend as the equilibrium selectivity, and is consistent with the observation in Figure 8. The increase in the C_2H_6 roll-up magnitude with a narrower pore-size distribution is largely due to the increase in the C_2H_6 micropore diffusivity caused by the increased adsorbate concentration of C_3H_8. For the conditions studied here, the variation in equilibrium adsorption with distribution variance is less pronounced compared with that from mean pore width, so the effect of micropore-size spread on the adsorption kinetics of C_3H_8 is not significant, as shown in Figure 9.

Conclusion

The proposed model has been successfully applied to predict the coadsorption of C_2H_6 and C_3H_8 on Ajax and Norit carbons at various conditions. The viscous flux in the macropore phase can be neglected without seriously affecting the prediction results for both adsorbates. The overshooting phenomena, occurring in the fast-diffusing/weak-adsorbing species in the mixture with slow-moving/strong-adsorbing compound, can be accurately predicted by this model for most of the conditions studied. It is found that generally the magnitude of the rollup for C_2H_6 increases with the increase in the ratio of C_3H_8 to C_2H_6 mole fraction, illustrating the influence of the dragging force exerted on C_2H_6 by C_3H_8. The model prediction is normally better for C_3H_8 than C_2H_6, indicating that the behavior of the lighter species C_2H_6 is affected more sensitively by C_3H_8 than vice versa. The model prediction for codesorption on both carbons is also very successful. The calculation for the displacement between C_2H_6 and C_3H_8 on Ajax carbon suggests that the adsorption or desorption of C_3H_8 dominates the displacement process, emphasizing the significance of the strong adsorbing component on the diffusion process of binary adsorbates. The success of the model prediction justifies the applicability of the MS method for describing the binary diffusivities in both the macropore and micropore phases. The deviation of model prediction from the experiment may be caused by the nonisothermal effect during adsorption, which needs further investigation. The parametric study of the effect of pore heterogeneity on adsorption kinetics suggests that the equilibrium selectivity of the heavier compound to the lighter one determines the magnitude of the rollup, reiterating the dominance of the heavier species in binary adsorption kinetics.

Acknowledgment

Support of this research by the Australian Research Council is gratefully acknowledged.

Notation

a = geometrical factor of the particle
b_i = ratio of adsorbate diffusion energy to heat of adsorption for species i
$C_{b,i}$ = bulk gas concentration of species i, mol·m^{-3}
$C_{me,i}$ = hypothetical gas-phase concentration of species i in pseudoequilibrium with micropore concentration, mol·m^{-3}
$C_{m,i}$,$C_{\mu t,i}$ = transient concentration in macropore and micropore phase of species i, mol·m^{-3}
$C_{\mu 0,i}$ = overall equilibrium adsorbate concentration of species i at bulk pressure, mol·m^{-3}
$C_{\mu,i}$ = local adsorbate phase concentration of species i in micropore of width H, mol·m^{-3}
C_i = amount adsorbed of species i, mol·m^{-3}
C_∞ = saturation capacity of the adsorbent, mol·m^{-3}
d_0 = macropore diameter, Å
$D_{\mu,i}$ = self-diffusivity of species i in adsorbate phase, m^2·s^{-1}
$D_{\mu,ij}$ = cross-diffusivity between species i and j in adsorbate phase, m^2·s^{-1}
$D_{\infty,i}$ = intrinsic adsorbate phase diffusivity of species i, m^2·s^{-1}

$D_{K,i}$ = Knudsen diffusivity of component i, $m^2 \cdot s^{-1}$
$D_{m,ij}$ = molecular diffusivity between components i and j, $m^2 \cdot s^{-1}$
$E_i(H)$ = adsorption potential energy of component i in micropore of width H, $J \cdot mol^{-1}$
$f(H)$ = pore-size distribution, $Å^{-1}$
$f_{a,i}$ = the transient fractional uptake of species i
H = micropore width, Å
$J_{m-\mu,i}$ = mass-transfer flux of species i between macropore and micropore phases, per unit volume, $mol \cdot m^{-3} \cdot s^{-1}$
$k_{a,i}(H)$ = local adsorption rate constant of species i in pore of width H, $mol \cdot m^{-2} \cdot s^{-1}$
$k_{d0,i}$ = desorption rate constant for species i in pore with zero adsorption energy, $m \cdot s^{-1}$
$k_{d\mu,i}(H)$ = local desorption rate constant for species i in micropore of width H, $m \cdot s^{-1}$
$k_{m,i}$ = mass-transfer coefficient of species i in outer surface of the particle, $m \cdot s^{-1}$
$[L]$ = matrix of the phenomenological adsorbate phase diffusivity
$[L_m]$ = matrix of the phenomenological macropore phase diffusivity
M_i = molecular weight of component i
$N_{p,i}^D, N_{p,i}^v$ = diffusive and viscous flux of species i in the adsorbate phase, $mol \cdot m^{-2} \cdot s^{-1}$
N_i = overall adsorbate phase flux of species i in the particle, $mol \cdot m^{-2} \cdot s^{-1}$
$\overline{N}_p$ = vector of local adsorbate phase flux in a single pore, $mol \cdot m^{-2} \cdot s^{-1}$
$\overline{N}_m$ = vector of macropore phase flux, $mol \cdot m^{-2} \cdot s^{-1}$
P = pressure, Pa
q = gamma distribution function parameter, $Å^{-1}$
R_0 = particle radius, m
R_g = universal gas constant, 8.314 $J \cdot mol^{-1} \cdot K^{-1}$
S_S = specific macropore surface area, m^{-1}
t = time, s
T = temperature, K
V_t^D = the diffusive velocity of species i in adsorbate phase, $m \cdot s^{-1}$
$y_{m,i}$ = mole fraction of species i in macropore phase
y_i = mole fraction of species i in the bulk phase
Z = radial position in particle
$Z_{m,i}$ = potential minimum distance from a surface plane of pore, Å)

Greek letters

δ_{kj} = Dirac delta function
δ_i = thermal expansion coefficient of species i, K^{-1}
ϵ_m, ϵ_μ = macroporosity and micropore porosity
$\phi_i(H)$ = potential energy in pore of width H, $J \cdot mol^{-1}$
γ = gamma function parameter
η_i = low-pressure viscosity of adsorbate i, $N \cdot s \cdot m^{-2}$
η_m = mixture viscosity in the macropore phase, $N \cdot s \cdot m^{-2}$
ν_i = site occupancy of adsorbate i
Δ = separation between graphite layers, Å
ϵ_{is} = solid–fluid interaction parameter, $J \cdot mol^{-1}$
Ω_i = diffusing volume of species i
σ_{is} = solid–fluid interaction parameter, Å
θ_i = local fractional coverage of species i
τ_m, τ_μ = macropore and micropore tortuosity

Subscripts

i,j,k = species

Matrix operations

$[\ ]^{-1}$ = inverse of a square matrix

Literature Cited

Bering, B. P., V. V. Serpinskii, and T. S. Yakubov, "Osmotic Theory of the Adsorption of Mixtures of Gases. 1. Integral of the Gibbs Equation and Isotherm of Adsorption," *Izv. Akad. Nauk SSSR, Ser. Khim.*, **4**, 727 (1977).

Bhatia, S. K., and L. P. Ding, "Vacancy Solution Theory of Adsorption Revisited," *AIChE J.*, **47**, 2136 (2001).

Chen, Y. D., and R. T. Yang, "Prediction Binary Fickian Diffusivities from Pure-Component Fickian Diffusivities for Surface Diffusion," *Chem. Eng. Sci.*, **47**, 3895 (1992).

Chen, Y. D., R. T. Yang, and L. M. Sun, "Further Work on Predicting Multicomponent Diffusivities from Pure-Component Diffusivities for Surface Diffusion and Diffusion in Zeolites," *Chem. Eng. Sci.*, **48**, 2815 (1993).

Chen, Y. D., R. T. Yang, and P. Uawithya, "Diffusion of Oxygen, Nitrogen and Their Mixtures in Carbon Molecular Sieve," *AIChE J.*, **40**, 577 (1994).

Cochran, T. W., R. L. Kabel, and R. P. Danner, "Vacancy Solution Theory of Adsorption Using Flory-Huggins Activity Coefficient Equations," *AIChE J.*, **31**, 268 (1985).

Coppens, M.-O., A. T. Bell, and A. K. Chakraborty, "Dynamic Monte-Carlo and Mean-Field Study of the Effect of Strong Adsorption Sites on Self-Diffusion in Zeolites," *Chem. Eng. Sci.*, **54**, 3455 (1999).

Delgado, J. A., and A. E. Rodrigues, "A Maxwell-Stefan Model of Bidisperse Pore Pressurization for Langmuir Adsorption of Gas Mixtures," *Ind. Eng. Chem. Res.*, **40**, 2289 (2001).

Ding, L. P., and S. K. Bhatia, "Vacancy Solution Theory for Binary Adsorption Equilibria in Heterogeneous Carbon," *AIChE J.*, **48**, 1938 (2002).

Ding, L. P., S. K. Bhatia, and F. Liu, "Kinetics of Adsorption on Activated Carbon: Application of Heterogeneous Vacancy Solution Theory," *Chem. Eng. Sci.*, **57**, 3909 (2002).

Do, D. D., and H. D. Do, "Non-Isothermal Effects on Adsorption Kinetics of Hydrocarbon Mixtures in Activated Carbon," *Sep. Purif. Technol.*, **20**, 49 (2000).

Do, H. D., and D. D. Do, "Maxwell-Stefan Analysis of Multicomponent Transient Diffusion in a Capillary and Adsorption of Hydrocarbons in Activated Carbon Particle," *Chem. Eng. Sci.*, **53**, 1239 (1998).

Hu, X., "Fundamental Studies of Multicomponent Adsorption, Desorption and Displacement Kinetics of Light Hydrocarbons in Activated Carbon," PhD Thesis, Univ. of Queensland, Brisbane, Australia (1992).

Kapteijn, F., J. A. Moulijn, and R. Krishna, "The Generalized Maxwell-Stefan Model for Diffusion in Zeolites: Sorbate Molecules with Different Saturation Loadings," *Chem. Eng. Sci.*, **55**, 2923 (2000).

Kärger, J., and M. Bülow, "Theoretical Prediction of Uptake Behavior in Adsorption Kinetics of Binary Gas Mixtures Using Irreversible Thermodynamics," *Chem. Eng. Sci.*, **30**, 893 (1975).

Kirkpatrick, S., "Percolation and Conduction," *Rev. Mod. Phys.*, **45**, 574 (1973).

Krichevskii, I. R., "Thermodynamic Foundations of the Adsorption of Gaseous Mixtures," *J. Phys. Chem. (USSR)*, **5**, 742 (1934).

Krishna, R., "Multicomponent Surface Diffusion of Adsorbed Species: A Description Based on the Generalized Maxwell-Stefan Equations," *Chem. Eng. Sci.*, **45**, 1779 (1990).

Krishna, R., "Problems and Pitfalls in the Use of the Fick Formulation for Intraparticle Diffusion," *Chem. Eng. Sci.*, **48**, 845 (1993a).

Krishna, R., "A Unified Approach to the Modeling of Intraparticle Diffusion in Adsorption Processes," *Gas Sep. Purif.*, **7**, 91 (1993b).

Krishna, R., and J. A. Wesselingh, "The Maxwell-Stefan Approach to Mass Transfer," *Chem. Eng. Sci.*, **52**, 861 (1997).

Marutovsky, R. M., and M. Bülow, "Sorption Kinetics of Multi-Component Gaseous and Liquid Mixtures on Porous Sorbents," *Gas Sep. Purif.*, **1**, 66 (1987).

Myers, A. L., and J. M. Prausnitz, "Thermodynamics of Mixed-Gas Adsorption," *AIChE J.*, **11**, 121 (1965).

Nitta, T., T. Shigetomi, M. Kuro-Oka, and T. Katayama, "An Adsorption Isotherm of Multi-Site Occupancy Model for Homogeneous Surface," *J. Chem. Eng. Jpn.*, **17**, 39 (1984).

Qiao, S., "Study of Multicomponent Adsorption Equilibrium and Kinetics of Hydrocarbons on Activated Carbon," PhD Thesis, Hong Kong Univ. of Science and Technology, Hong Kong (2000).

Qiao, S., and X. Hu, "Use Iast with Mpsd to Predict Binary Adsorption Kinetics on Activated Carbon," *AIChE J.*, **46**, 1743 (2000).

Rao, M. B., and S. Sircar, "Thermodynamic Consistency for Binary Gas Adsorption Equilibria," *Langmuir*, **15**, 7258 (1999).
Reid, R. C., J. M. Prausnitz, and B. E. Poling, *The Properties of Gases and Liquids*, McGraw-Hill, New York (1987).
Sanborn, M. J., and R. Q. Snurr, "Predicting Membrane Flux of Ch_4 and Cf_4 Mixtures in Faujasite from Molecular Simulations," *AIChE J.*, **47**, 2032 (2001).
Saravanan, C., and S. M. Auerbach, "Modeling the Concentration Dependence of Diffusion in Zeolites. Ii. Kinetic Monte Carlo Simulations of Benzene in Na-Y," *J. Chem. Phys.*, **107**, 8132 (1997).
Steele, W. A., "The Physical Interaction of Gases with Crystalline Solids," *Surf. Sci.*, **36**, 317 (1973).
Sundaram, N., and R. T. Yang, "Binary Diffusion of Unequal Sized Molecules in Zeolites," *Chem. Eng. Sci.*, **55**, 1747 (2000).
Suwanayuen, S., and R. P. Danner, "Vacancy Solution Theory of Adsorption from Gas Mixtures," *AIChE J.*, **26**, 76 (1980).
Talu, O., and A. L. Myers, "Letter to the Editor," *AIChE J.*, **34** 1931 (1988).
Villadsen, J. V., and W. E. Stewart, "Solution of Boundary-Value Problems by Orthogonal Collocation," *Chem. Eng. Sci.*, **22**, 1483 (1967).
Wang, K., "The Effect of Microporous Structure on Adsorption Equilibria and Kinetics on Activated Carbon," PhD Thesis, Univ. of Queensland, Brisbane, Australia (1998).
Wang, K., and D. D. Do, "Multicomponent Adsorption, Desorption and Displacement Kinetics of Hydrocarbons on Activated Carbon-Dual Diffusion and Finite Kinetics Model," *Sep. Purif. Technol.*, **17**, 131 (1999).
Yakubov, T. S., B. P. Bering, and V. V. Serpinskii, "Osmotic Theory of the Adsorption of Mixtures of Gases. 2. General Equation of the Adsorption Isotherm of Gas Mixtures," *Izv. Akad. Nauk SSSR, Ser. Khim.*, **5**, 991 (1977).
Yang, R. T., *Gas Separation by Adsorption Processes*, Imperial College Press, London (1997).
Yang, R. T., Y. D. Chen, and Y. T. Yeh, "Prediction of Cross-Term Coefficients in Binary Diffusion: Diffusion in Zeolite," *Chem. Eng. Sci.*, **46**, 3089 (1991).

Manuscript received Mar. 8, 2002, and revision received Sept. 17, 2002.